Implantable, multifunctional, bioresorbable optics

Hu Tao[a,1], Jana M. Kainerstorfer[a,1], Sean M. Siebert[a], Eleanor M. Pritchard[a], Angelo Sassaroli[a], Bruce J. B. Panilaitis[a], Mark A. Brenckle[a], Jason J. Amsden[a], Jonathan Levitt[b], Sergio Fantini[a], David L. Kaplan[a,c], and Fiorenzo G. Omenetto[a,d,2]

[a]Department of Biomedical Engineering, Tufts University, Medford, MA 02155; [b]Department of Physics of Complex Systems, Weizmann Institute of Science, Rehovot 76100, Israel; [c]Department of Chemical and Biological Engineering, Tufts University, Medford, MA 02155; and [d]Department of Physics and Astronomy, Tufts University, Medford, MA 02155

Advances in personalized medicine are symbiotic with the development of novel technologies for biomedical devices. We present an approach that combines enhanced imaging of malignancies, therapeutics, and feedback about therapeutics in a single implantable, biocompatible, and resorbable device. This confluence of form and function is accomplished by capitalizing on the unique properties of silk proteins as a mechanically robust, biocompatible, optically clear biomaterial matrix that can house, stabilize, and retain the function of therapeutic components. By developing a form of high-quality microstructured optical elements, improved imaging of malignancies and of treatment monitoring can be achieved. The results demonstrate a unique family of devices for in vitro and in vivo use that provide functional biomaterials with built-in optical signal and contrast enhancement, demonstrated here with simultaneous drug delivery and feedback about drug delivery with no adverse biological effects, all while slowly degrading to regenerate native tissue.

biomedical optics | silk optics | biophotonics

The use of biocompatible materials is paramount for biomedical applications in supports, casings, or implants needed to integrate within the human body to minimize immune responses. Polymers such as polylactic acids (1, 2) and collagens (3) have been widely studied as implantable, resorbable biomaterial matrices for a range of current or potential medical device needs. Toward this goal, recent interest in integrating the favorable biological interface attributes of biomaterials with technological functionalities such as electronics (4) or optics (5) provides a new and exciting path toward integrating devices within living tissue and eliminating the need for retrieval after their functional lifetimes are complete. For this approach to be viable, the polymer must meet the required material tolerances to favorably compare with common technical substrates such as glass, plastics, or (inorganic) polymers. These requirements present a significant barrier to success because mechanical demands, optical clarity requirements, and reliable electronic interfaces, among many other environmental impacts and insults, establish a range of material performance issues that are difficult to achieve. When further challenged by the needs for degradability and safety for tissue regeneration, the barriers to success only grow.

Recent results indicate that silk possesses a convenient convergence of the individual features outlined above, suggesting a path forward with this unique protein biomaterial. Silk is already a widely used biopolymer approved by the US Department of Agriculture (6). Further, silk has been shown to be suitable for use as a material platform for sophisticated optical and opto-electronic components with features on the micro- and nanoscale (7–9). The resulting free-standing devices formed from silk are refractive or diffractive and comprise elements ranging from microlens arrays and white-light holograms to diffraction gratings and planar photonic crystals with minimum feature sizes of less than 20 nm (7, 9, 10). These components provide mechanically stable, high-quality optical elements that are fully degradable, biocompatible, and implantable (11). Additionally, silk materials have been shown to possess the ability to entrain and stabilize labile biological components (12–14), which provides the opportunity for functionalized

optical devices, such as for drug delivery. In the present work, we demonstrate the confluence of optical form and biomedical function in one system, by manufacturing implantable, multifunctional, bioresorbable micro-optical devices. The results demonstrate a next-generation concept that has reached reality and opens the door to new medical device designs that can have an impact on health care in many modes.

Free-standing 2D microprism arrays (MPAs) prepared solely from purified/reconstituted silk protein serve as the optical platform in the present study. This system provides optical signal and contrast enhancement by retroreflecting forward-scattered photons through layers of tissue, causes no adverse biological effects, and is slowly degraded and integrated into native tissue in vivo. Optical signal and contrast enhancement allow for improved noninvasive imaging of tissue. Additionally, the utility of the silk MPAs is augmented by incorporating biochemical function to demonstrate multifunctional optical elements. To demonstrate that the enhanced reflectivity of this device is not compromised by functionalizing the silk MPA, dopants have been included in the silk material, which in this work are either gold nanoparticles (AuNPs) or the chemotherapeutic drug doxorubicin. Furthermore, the resulting functional silk microreflector device doped with doxorubicin not only shows enhanced reflectivity offered by the optical device but also allows for storage, controlled delivery, and imaging of therapeutics. The optical performance of the reflector provides important transduction and monitoring mechanisms; changes in reflectivity of the dissolving device can be correlated to the amount of drug eluted.

Silk MPAs were prepared by using micromolding techniques akin to soft lithography by replicating a microprism array master mask, resulting in a 100-μm-thick, free-standing silk reflector film with dimensions up to tens of square centimeters (Fig. 1A and *SI Appendix*, Figs. S1 and S2). The dissolution time of the MPA films can be tuned by controlling the degree of crystallinity during the silk protein self-assembly process by regulating the water content within the film through an annealing step (15–17). This approach can be used to allow rapid to slow degradation of the device, depending on the application (*SI Appendix*, Fig. S3). In the case of doxorubicin, drug delivery can be achieved in a localized and controlled fashion.

The utility of this passive optical device is to increase the amount of light (specifically, near-infrared light between 600–1,000 nm) that returns to a detector situated at the surface of a biological specimen when the reflector film is introduced underneath the specimen. An implantable silk MPA embedded in tissue could
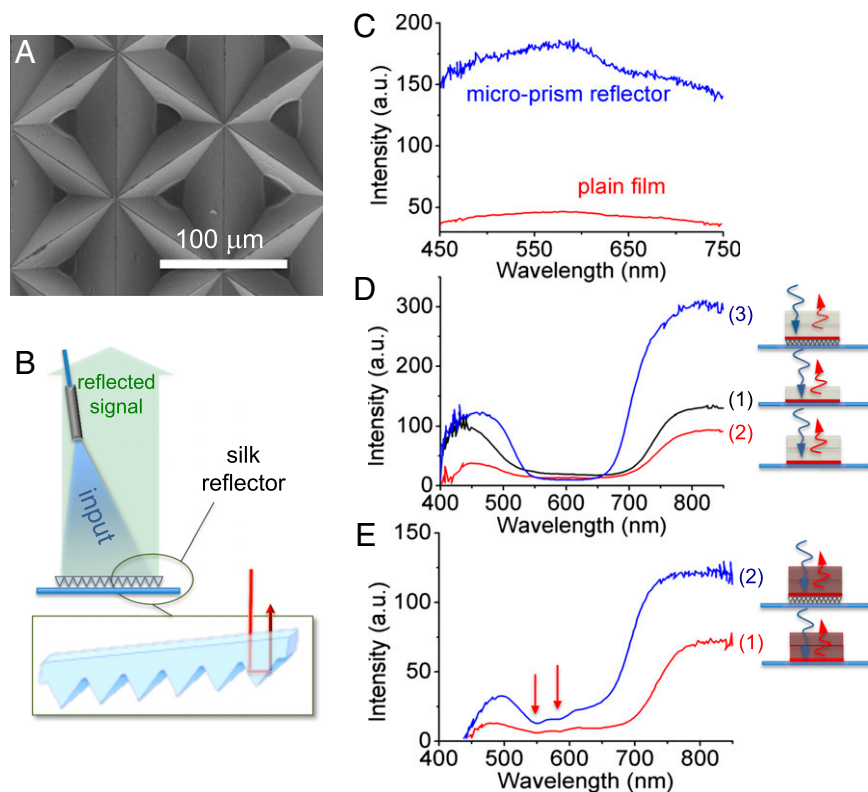
Fig. 1. (*A*) Scanning electron microscope image of a silk microprism array (MPA). (*B*) The schematic of the experimental setup for the evaluation of the performance of a replicated MPA. Incoherent white-light illumination was provided to the silk reflector from a fixed height and a backscattering reflection probe is used to collect the response from the same height and couple it to a spectrometer. (*C*) The silk MPA shows significant increase in reflected signal compared with the unpatterned plain film. (*D* and *E*) Results from in vitro experiments from tissue layers characterized with the setup shown in *B*, where a silk MPA is placed underneath a spectrally responsive element, a layer of cellulose embedded with red pigment, to capture scattered photons in the forward direction and enhanced the backscattered signal. (*D*) Comparison between the signal detected from (*1*) the spectral element covered by one layer of fat, (*2*) the same covered by two fat layers, and (*3*) the same as in (*2*) but with the silk MPA under the spectral element. The reflectivity response was significantly higher when the mirror was present. The same experiment was repeated by using layers of muscle tissue. The data are presented in *E* that compare (*1*) the response due to the spectral element covered with two layers of muscle tissue with (*2*) the same with the reflector in place. The arrows indicate the absorption peaks of the tissue.

capture forward-scattered photons that are ordinarily lost in reflection-based imaging techniques (18, 19). This would enhance intrinsic sensitivity for measurement over thicknesses where dimensions normally exceed typical photon mean free paths (MFP, $l = \frac{1}{(\mu_a + \mu_s)}$; μ_a, absorption coefficient and μ_s, scattering coefficient; $\mu_s \gg \mu_a$ for most tissues) without resorting to coherent detection techniques or contrast agents for image enhancement. Not only does this performance allow for enhanced signal for deep-tissue imaging, but it should also allow for contrast enhancement, which is of even greater importance, because imaging of deep-tissue malignancies is not necessarily limited by detection of light, but rather by contrast to the surrounding tissue. Hence, contrast enhancement is of great importance for improved imaging of malignancies.

To validate the optical performance of the enhanced signal using MPAs, diffuse reflected light from the silk MPAs was monitored under isotropic illumination of tissuelike phantoms. For imaging of shallower depth (i.e., for subcutaneous applications), a colocalized source and detection unit was used (Fig. 1*B*). For imaging deeper tissue, the geometry of the fiber-based backscattering imaging setup (Fig. 2 *A* and *D*) was such that a broadband light source was used for illumination and a detection fiber was scanned over the phantom, leading to illumination source–detector distances between 8–38 mm, in 2-mm increments, which allowed for probing multiple tissue depths.

The presence of the reflector resulted in a significant enhancement of signal at the detector plane, increasing the backscattered signal intensity by nearly fivefold compared with an unpatterned silk film (Fig. 1*C*) and by two orders of magnitude compared with background (*SI Appendix*, Figs. S4 and S5).

For s.c. applications, an in vitro experiment was performed to assess the variation in optical response caused by the presence of the MPA by placing the device under a layer of cellulose embedded with red pigment. The MPA reflector and cellulose combination was covered by single or multiple layers of 800-μm-thick porcine fat (Fig. 1*D*) or by single or multiple layers of muscle tissue (Fig. 1*E*). As expected, in the absence of MPAs the detected spectral response was progressively attenuated as layers of fat or muscle tissue were stacked on the device. The presence of the silk reflector underneath the fat structure significantly enhanced the backscattered signal collected and its dynamic range, allowing collection of the spectral response of the embedded pigmented layer (*SI Appendix*, Fig. S6). A similar response was observed when using muscle tissue, where the presence of the silk MPA causes an increase in the dynamic range of the detected signal, revealing the spectral signature of myocytes with absorption peaks appearing at $\lambda_1 \sim 550$ nm and $\lambda_2 \sim 575$ nm. Additional experiments are presented in *SI Appendix*, Figs. S7 and S8).

For demonstrating the potential for enhanced deep-tissue imaging, experiments were performed on solid delrin phantoms (Fig. 2), which are highly scattering and mimic well the scattering
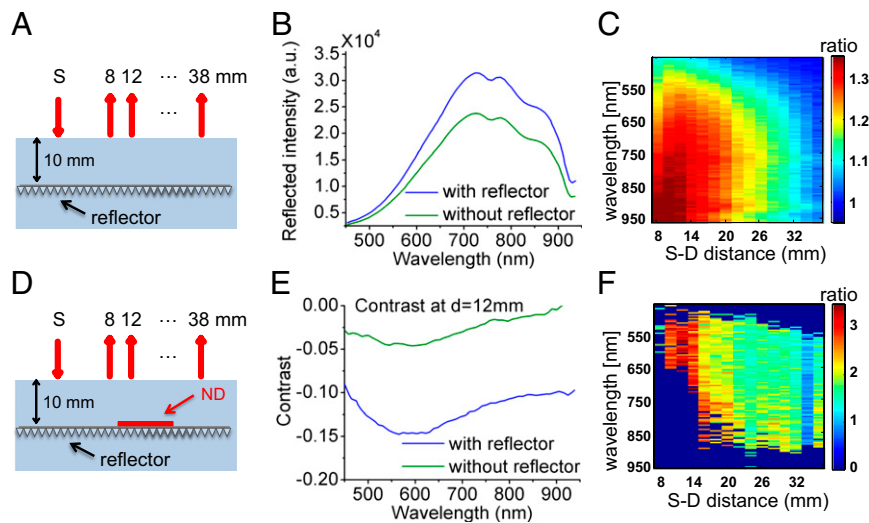
Fig. 2. Phantom results for demonstrating signal and contrast enhancement with the MPAs in deep tissue. (*A*) The schematic of the experimental setup with a variable source–detector separation for imaging deeper layers. Illumination was provided to the phantom, with the fiber tip touching the phantom surface. The detection fiber is scanned along the phantom and the reflector is placed in a depth of 1 cm. The detection fiber was coupled to a spectrometer. (*B*) The MPA shows significant increase in reflected signal compared with measuring reflectance from the phantom alone. (*C*) This increase in signal reduces with larger source–detector distances. (*D*) Scanning geometry for contrast imaging. For contrast measurements, an 8 × 8-mm ND filter is additionally put on top of the reflector, mimicking a local inclusion. (*E*) The contrast enhancement for measuring the ND filter is increased 3.5 times at source–detector distance of 12 mm and also decreases with larger separations (*F*), still showing a two times increase at 20 mm.

in tissue, as well as liquid phantoms, which were made of a milk, water, and ink mixture, mimicking not only scattering, but also absorption in tissue (*SI Appendix*, Fig. S9).

For determining the signal enhancement at 1-cm depth, imaging was performed on the phantom alone and with the MPA embedded at 1-cm depth. The presence of the reflector inside the delrin phantom resulted in a significant enhancement of signal at the detector plane, increasing the backscattered signal intensity 1.4 times at source–detector distances of ~12 mm compared with the phantom alone (Fig. 2*B*). The ratio between intensity with reflector and phantom alone can be seen in Fig. 2*C* for all source–detector separations. In the case of the liquid phantom (*SI Appendix*, Fig. S9), which includes ink as an absorbing material, the enhancement is still significant (~20%), even at 1-cm depth.

Because diagnostics depend on differences between healthy and malignant tissue, contrast is of crucial importance. To determine contrast enhancement at 1-cm depth, an 8- × 8-mm neutral density (ND) filter (OD = 0.6) was used to mimic a local inclusion (Fig. 2*D*). Imaging was performed with the ND filter on top of the reflector as well as with the ND filter alone. Contrast was defined as the $(I - I_0)/I_0$, where I is the measured reflected intensity with the ND filter at 1 cm and I_0 is the background intensity without the reflector. A 3.5-times increase in contrast was found (Fig. 2*E*) at a source–detector distance of 12 mm. The contrast enhancement for all source–detector distances can be found in Fig. 2*F*. Contrast enhancement in 1-cm depth of the liquid phantom (*SI Appendix*, Fig. S10) was reduced in comparison with the delrin phantom but was still 2.5 times larger in comparison with no embedded reflector.

These in vitro results provided initial validation of the silk MPA performance in an in vitro environment and its utility for improved imaging. To support the applicability of the concept as an implantable device, in vivo studies were conducted by implanting the silk MPA structures in BALB/c mice (Fig. 3*A* and *B*) in accordance with approved protocols. All animal research at Tufts University, including those presented here, are reviewed and approved by the Institutional Animal Care and Use Committee prior to initiation. Two samples, one flat silk and one micropatterned MPA silk film (both 100 µm thick, ~1 × 1 cm) were inserted s.c. after ethylene

oxide sterilization through an incision on the back of the mice. After suturing the wound site, the scattered signal was measured with the colocalized imaging geometry (*n* = 3; *SI Appendix*, Fig. S11). The backscattered illumination through the mouse skin was collected by a fiber probe at the implant site, and a threefold improvement (Fig. 3*C*) in collected signal was measured with the MPA in comparison with the control areas (mouse skin where either a flat film or no film was present) (*SI Appendix*, Fig. S12).

Further substantiation of the MPA performance was carried out using a Monte Carlo code to solve the radiative transfer equation, an integro-differential equation widely used for describing light propagation in random media such as biological tissues (20). The approach was used to calculate the backscattered signal intensity in the presence of the silk MPA reflector. In this simulation, the silk device was postulated to provide 100% reflectivity and to be located at a depth of 0.6 mm under the skin surface with a scattering coefficient of $\mu_s = 12$ mm^{-1} and an absorption coefficient of $\mu_a = 0.01$ mm^{-1}, typical of skin and muscle tissues in the near-infrared wavelength range (650–850 nm) (21), showing a predicted increase in reflected signal in agreement with what is observed experimentally (~3× reflectivity enhancement) (*SI Appendix*, Fig. S13).

The reflector performance was monitored in the same mice 2 wk after implantation. The measured signal enhancement was found to be lower than the initial value (~2× reflectivity enhancement; *SI Appendix*, Fig. S16) because of enzymatic degradation and initial remodeling and reintegration of the MPA in the native tissue, as designed. This process directly affects the optical quality of the implant. The devices were also monitored for adverse reactions and resorbability by histopathological sections of the implanted silk film and the underlying tissue. No visible inflammation was found at 2 wk after implantation, and initial evidence suggesting reincorporation into the tissue matrix, such as revascularization on the surface of the film (*SI Appendix*, Fig. S14), was observable upon examination of flat films after 4 wk of implantation by examining the excised tissue. It was also still possible to identify the microprism arrays in the histological sections (*SI Appendix*, Figs. S15 and S20).

Whereas the optical utility alone provides a demonstration of in vivo integration of these optical devices within living tissue and improved imaging capabilities, additional advantages are present
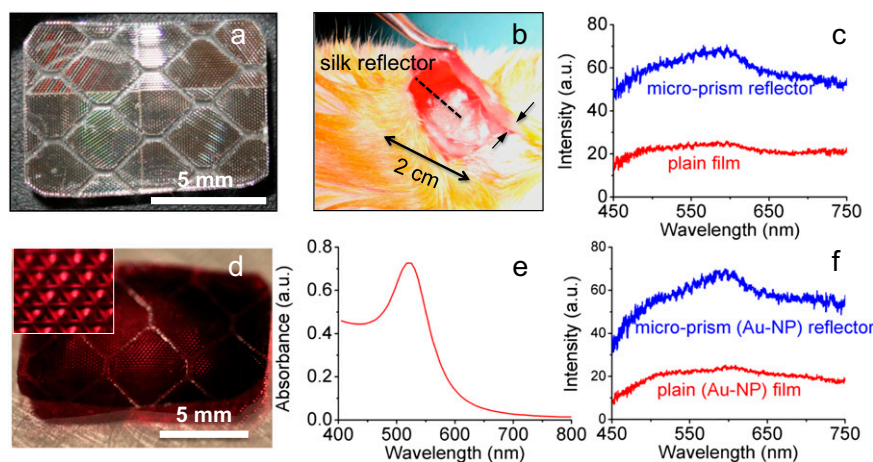
Fig. 3. In vivo results from the use of silk MPAs and Au-NP MPAs. (*A*) The MPAs for implantation were prepared with a size of ~1 × 1 cm. (*B*) The s.c. implantation of a silk MPA in the dorsal region of a mouse. (*C*) The backscattered signal was measured in vivo and shows ~3× enhancement due to the MPA right after implantation. (*D*) Au-NP–doped silk MPAs with dimensions of ~1 × 1 cm were prepared for implantation. (*E*) The Au-NP–silk solution, which was used to cast MPAs, show enhanced absorption due to the Au-NP doping, as illustrated in (*F*). The backscattered signal of the implanted silk MPA was measured and compared with a control signal taken from an Au-NPs–doped flat (e.g., unpatterned) silk film also implanted in the mouse's dorsal region as a control. The measurement shows signal enhancement similar to that of the undoped counterparts in *C*.

at the union of form and function enabled by the silk biomaterial platform with incorporated dopants. This integrate of active moieties generates doped silk MPAs with additional biomedical relevance beyond enhanced optical imaging. To demonstrate that the imaging capabilities of such functionalized MPA can be maintained, silk MPAs were prepared with a silk Au-NP solution. The Au-NPs, prepared according to published protocols (22), were mixed in the silk solution, which was subsequently cast on the previously used microprism masters, yielding free-standing Au-NP–silk MPAs (Fig. 3*D*). Similarly to gold nanoshells, Au-NPs resonantly absorb specific wavelengths (Fig. 3*E*) of incident light and convert this energy to heat. This technique has been successfully used in phototherapy for in vivo medical applications, such as to treat infections (23), tumor mitigation (24), and pain relief (25). The resulting Au-NP silk microprism reflectors were implanted in mice, alongside control Au-NP–doped flat films, following the same procedures previously described. The in vivo measurements at 0 wk (Fig. 3*F*) and 2 wk (*SI Appendix*, Fig. S16) after implantation display similar optical performance, which is three times signal enhancement compared with plain film, to what was previously observed for the undoped devices by enhancing the diffuse reflective signal (*n* = 3; *SI Appendix*, Fig. S16). Hence, the doped film does not change the bulk signal enhancement. However, a detectable difference in the in vitro spectral response caused by the absorption of the Au-NPs entrained within the silk matrix (*SI Appendix*, Fig. S17) was found. Because the absorption spectra are changed in comparison with a plain film and are specific to the Au-NP, the doped MPA become functionalized, and the optical performance of the device can be tuned by the Au-NP MPAs localized light-absorbing patches. This can be demonstrated by illuminating the mice with green laser light to match the absorption peak of the Au-NPs entrained in the film (*SI Appendix*, Fig. S18). A green laser beam (Coherent Verdi 10) of initial diameter $w_0 = 3$ mm is expanded to a diameter of w ~5 cm, corresponding to an irradiance of ~0.13 W/cm^2 to cover the back of the Balb-c mouse. A thermal image (SC645; FLIR) of the mouse shows an area of increased temperature (ΔT ~5 °C) at the implant site corresponding to the s.c. Au-NP mirror (*SI Appendix*, Fig. S19). This localized temperature increase is also used to demonstrate in vitro the elimination of bacteria by placing Au-NP MPAs in contact with a bacterial lawn and illuminating with green light (*SI Appendix*, Figs. S18 and S19). For the in vivo samples, as before, histopathological sections of the

Au-NP MPAs and Au-NP–doped films revealed no inflammatory response, encapsulation, or fibrosis after 2 wk of implantation (*SI Appendix*, Fig. S20). In the case of the silk Au-NP MPA, optical enhancement and plasmon absorption from the Au-NP provide independent functions within the same implantable device without reducing the functionality of either.

A promising opportunity for such doped MPA is to add therapeutic functionality and have the entrained dopant modulate optical performance of the device (10). Silk is a particularly promising platform that has been shown to work as a biomaterial matrix to stabilize a range of compounds, including monoclonal antibodies, antibiotics, and vaccines (26). Specifically, we explore combining the capacity of silk materials to stabilize entrained labile compounds by colocating them in the same device. This device can provide drug stabilization and controlled drug delivery while simultaneously providing an optical feedback of delivery. Common approaches for drug delivery can be roughly divided into two groups. The first group consists of small-scale implantable systems for sustainable, long-term drug release (27), which most commonly lack the ability to provide feedback of drug delivered. The second group focuses on targeted drug delivery (i.e., with functionalized nanoparticles) (28), where the drug delivery mechanism is a burst release. In the latter case, optical monitoring of drug release can be achieved by triggering not only the release (i.e., binding to the cell surface receptor) but also a fluorescent marker (29, 30). Another approach for imaging and treating at the same time is using fluorescence lifetime for tumor receptor quantification (31). However, in this case, treatment is not achieved simultaneously with imaging. For the approach presented here, no additional compound for triggering of the release is necessary, because the degradation of the MPA is controlling the release, and sustainable, long-term release can be achieved as well. Most importantly, the optical performance of the device should degrade with the degradation of the device, hence allowing for quantification of drug release in real time over the full time period of release.

Hence, the implantable optical device can serve its therapeutic function and changes in reflectivity would be related to the amount of drug eluted and used, as a drug delivery monitoring mechanism. To this end, we used doxorubicin (DxR), a therapeutic dopant commonly used in the treatment of a wide range of cancers, including many types of carcinomas and soft-tissue sarcomas. DxR was added to the silk solution, which was then reformed into free-

ENGINEERING

APPLIED BIOLOGICAL SCIENCES

standing DxR silk microprism films. The performance of the silk DxR MPA was evaluated in vitro to correlate the quantity of eluted drug with changes in reflectivity of the MPA. The silk DxR MPAs were immersed in a broad-spectrum serine proteinase solution (proteinase k with a concentration of 0.1 mg/mL; *SI Appendix*, Fig. S21 and Table S1) to mimic the degradation process that the devices would be subject to in an in vivo environment. The silk DxR MPA was evaluated at different time points for optical performance and drug content eluted by measuring absorbance at 495 nm and comparing measured values to a standard curve (Fig. 4*A* and *SI Appendix*, Fig. S22). The resulting curves were compared with the reflectivity of the silk DxR MPA at different time points, to show the relationship between drug released and the measured MPA reflectivity (with a correlation coefficient $\rho = 0.98$). The changes in reflectivity from the MPAs follow both the burst release and the sustained-release phase. The drug release in this case was predominantly degradation-mediated (i.e., drug only releases as the film degrades). The signal decrease as a function of microprism degradation also substantiates previous observations from the undoped silk MPAs and is further corroborated by inspecting the

silk DxR MPA at different stages of incubation in the proteinase buffer (0, 6, and 30 h) that show the degradation of the microprism structure (Fig. 4*B*). Additionally, these devices possess the ability to store and maintain the efficacy of DxR. The DxR-loaded silk MPAs were stored at −20 °C (frozen) and 60 °C for 3 wk, after which it was determined that the fluorescence of the DxR stored in silk films did not significantly decrease, despite the 80 °C range in storage temperature, in relation to comparable samples in solution (Fig. 4 *C* and *D* and *SI Appendix*, Figs. S23 and S24). These results demonstrate the multifunctionality of the device, from optical enhancement for imaging, to drug storage, to optical monitoring and quantification of drug delivery in real time and over the entire time period of release.

The results presented here enable new classes of optical devices that become fully integrated into regenerated tissues over time after their imaging utility is exhausted, eliminating the need for retrieval and extending the utility of in vivo screening modalities. Silk proves to be a particularly favorable material for these needs because it provides a convenient connection of material form and biological function. The ability to control the material degradation

Fig. 4. Multifunctional optical device. Chemotherapeutic, doxorubicin-loaded silk reflectors (DxR MPAs) are characterized in vitro under enzymatic degradation (proteinase k with a concentration of 0.1 mg/mL). (*A*) The drug release (*Upper*) and the reflectivity of the DxR MPAs (*Lower*) and the optical microscope image of a portion of the DxR-doped microprisms (*Inset*). The data are collected during the burst release (hourly up to 6 h) and during the sustained-release phase (every 6 h up to 30 h) (*n* = 6). (*B*) SEM images of DxR-MPA structures at 0, 6, and 30 h, showing a gradual breakdown of the microprisms due to the enzymatic degradation. (Scale bar, 50 μm.) (*C*) A comparison between DxR dissolved in ultrapure water and DxR-loaded silk MPAs (both with a concentration of 0.8 mg/mL) after storage at −20 °C and 60 °C for 3 wk. The silk DxR MPA maintains the fluorescence of the DxR after 3 wk at 60 °C in contrast to the solution. (*D*) The DxR MPAs were then fully degraded with 10 mg/mL proteinase k solution and were compared with the DxR solution by measuring the fluorescence intensity (excitation = 430 nm, emission = 550 nm) to determine the chemical activity of the drug. DxR fluorescence decreases when stored in solution, whereas the fluorescence of the DxR stored in MPAs does not significantly decrease with the 80 °C increase in storage temperature (two-tailed *P* value: $P < 0.02$ at −20 °C and $P < 0.001$ at 60 °C, Student *t* test).

properties (32) and reform silk biopolymers into technological formats adds opportunity for devices that can seamlessly operate at the nexus of enhanced imaging (through optical transduction), therapy (through drug stabilization and delivery), and quantitative feedback of therapy (through drug-delivery imaging within the same device).

The results bear particular promise given the implications of individualized monitoring of drug delivery in vivo and the concepts for multifunctional devices, where a single device can administer a cure while providing information of disease progression. The utility of multifunctional bioresorbable devices goes beyond medical applications into environmental monitoring or food safety, where such devices could be used without negative impact on the environment or the consumer.

1. Howard D, et al. (2002) Immunoselection and adenoviral genetic modulation of human osteoprogenitors: In vivo bone formation on PLA scaffold. *Biochem Biophys Res Commun* 299(2):208–215.
2. Partridge K, et al. (2002) Adenoviral BMP-2 gene transfer in mesenchymal stem cells: In vitro and in vivo bone formation on biodegradable polymer scaffolds. *Biochem Biophys Res Commun* 292(1):144–152.
3. Stone KR, Steadman JR, Rodkey WG, Li ST (1997) Regeneration of meniscal cartilage with use of a collagen scaffold. Analysis of preliminary data. *J Bone Joint Surg Am* 79A(12):1770–1777.
4. Kim DH, et al. (2010) Dissolvable films of silk fibroin for ultrathin conformal bio-integrated electronics. *Nat Mater* 9(6):511–517.
5. Parker ST, et al. (2009) Biocompatible silk printed optical waveguides. *Adv Mater* 21 (23):2411–2415.
6. Altman GH, et al. (2003) Silk-based biomaterials. *Biomaterials* 24(3):401–416.
7. Amsden JJ, et al. (2010) Rapid nanoimprinting of silk fibroin films for biophotonic applications. *Adv Mater* 22(15):1746–1749.
8. Lawrence BD, Cronin-Golomb M, Georgakoudi I, Kaplan DL, Omenetto FG (2008) Bioactive silk protein biomaterial systems for optical devices. *Biomacromolecules* 9(4): 1214–1220.
9. Perry H, Gopinath A, Kaplan DL, Dal Negro L, Omenetto FG (2008) Nano- and micropatterning of optically transparent, mechanically robust, biocompatible silk fibroin films. *Adv Mater* 20(16):3070–3072.
10. Domachuk P, Perry H, Amsden JJ, Kaplan DL, Omenetto FG (2009) Bioactive "self-sensing" optical systems. *Appl Phys Lett* 95(25):253702–253702-3.
11. Omenetto FG, Kaplan DL (2008) A new route for silk. *Nat Photonics* 2(11):641–643.
12. Wilz A, et al. (2008) Silk polymer-based adenosine release: Therapeutic potential for epilepsy. *Biomaterials* 29(26):3609–3616.
13. Pritchard EM, Kaplan DL (2011) Silk fibroin biomaterials for controlled release drug delivery. *Expert Opin Drug Deliv* 8(6):797–811.
14. Szybala C, et al. (2009) Antiepileptic effects of silk-polymer based adenosine release in kindled rats. *Exp Neurol* 219(1):126–135.
15. Lu Q, et al. (2010) Water-insoluble silk films with silk I structure. *Acta Biomater* 6(4): 1380–1387.
16. Hu X, et al. (2011) Regulation of silk material structure by temperature-controlled water vapor annealing. *Biomacromolecules* 12(5):1686–1696.
17. Jin HJ, et al. (2005) Water-stable silk films with reduced beta-sheet content. *Adv Funct Mater* 15(8):1241–1247.

18. Matcher SJ, Cope M, Delpy DT (1997) In vivo measurements of the wavelength dependence of tissue-scattering coefficients between 760 and 900 nm measured with time-resolved spectroscopy. *Appl Opt* 36(1):386–396.
19. Zonios G, Dimou A (2009) Light scattering spectroscopy of human skin in vivo. *Opt Express* 17(3):1256–1267.
20. Ishimaru A (1991) Wave propagation and scattering in random media and rough surfaces. *Proc IEEE* 79(10):1359–1366.
21. Calabro K, Curtis A, Galarneau JR, Krucker T, Bigio IJ (2011) Gender variations in the optical properties of skin in murine animal models. *J Biomed Opt* 16(1):011008.
22. Liang ZQ, et al. (2007) A centrifugation-based method for preparation of gold nanoparticles and its application in biodetection. *Int J Mol Sci* 8(6):526–532.
23. Huang WC, Tsai PJ, Chen YC (2007) Functional gold nanoparticles as photothermal agents for selective-killing of pathogenic bacteria. *Nanomedicine-UK* 2(6):777–787.
24. O'Neal DP, Hirsch LR, Halas NJ, Payne JD, West JL (2004) Photo-thermal tumor ablation in mice using near infrared-absorbing nanoparticles. *Cancer Lett* 209(2):171–176.
25. Jaeger GT, Larsen S, Soli N, Moe L (2007) Two years follow-up study of the pain-relieving effect of gold bead implantation in dogs with hip-joint arthritis. *Acta Vet Scand* 49(9):31–38.
26. Guziewicz N, Best A, Perez-Ramirez B, Kaplan DL (2011) Lyophilized silk fibroin hydrogels for the sustained local delivery of therapeutic monoclonal antibodies. *Biomaterials* 32(10):2642–2650.
27. LaVan DA, McGuire T, Langer R (2003) Small-scale systems for in vivo drug delivery. *Nat Biotechnol* 21(10):1184–1191.
28. Liu Y, Miyoshi H, Nakamura M (2007) Nanomedicine for drug delivery and imaging: a promising avenue for cancer therapy and diagnosis using targeted functional nanoparticles. *Int J Cancer* 120(12):2527–2537.
29. Kim M, et al. (2012) Real-time monitoring of anticancer drug release in vitro and in vivo on titania nanoparticles triggered by external glutathione. *Talanta* 88:631–637.
30. Weinstain R, Segal E, Satchi-Fainaro R, Shabat D (2010) Real-time monitoring of drug release. *Chem Commun (Camb)* 46(4):553–555.
31. Ardeshirpour Y, et al. (2011) Using in-vivo fluorescence imaging in personalized cancer diagnostics and therapy, an image and treat paradigm. *Technol Cancer Res Treat* 10(6):549–560.
32. Wang Y, et al. (2008) In vivo degradation of three-dimensional silk fibroin scaffolds. *Biomaterials* 29(24-25):3415–3428.

ENGINEERING

APPLIED BIOLOGICAL SCIENCES